Biosensors and Bioelectronics 33 (2012) 267–273

Contents lists available at SciVerse ScienceDirect

Biosensors and Bioelectronics

journal homepage: www.elsevier.com/locate/bios

Using the nanoimprint-in-metal method to prepare corrugated metal structures for plasmonic biosensors through both surface plasmon resonance and index-matching effects

Chen-Chieh Yu, Kuan-Hung Ho, Hsuen-Li Chen*, Shang-Yu Chuang, Shao-Chin Tseng, Wei-Fang Su

Department of Materials Science and Engineering, National Taiwan University, No. 1, Sec. 4, Roosevelt Road, Taipei 10617, Taiwan

ARTICLE INFO

Article history:
Received 14 October 2011
Received in revised form 3 January 2012
Accepted 17 January 2012
Available online 24 January 2012

Keywords:
Nanoimprint-in-metal
Corrugated metal structure
Biosensor
Surface plasmon resonance
Index-matching effect

ABSTRACT

In this study, we prepared metallic corrugated structures for use as highly sensitive plasmonic sensors. Relying on the direct nanoimprint-in-metal method, fabrication of this metallic corrugated structure was readily achieved in a single step. The metallic corrugated structures were capable of sensing both surface plasmon resonance (SPR) wavelengths and index-matching effects. The corrugated Au films exhibited high sensitivity (ca. 800 nm/RIU), comparable with or even higher than those of other reported SPR-based sensors. Because of the unique index-matching effect, refractometric sensing could also be performed by measuring the transmission intensity of the Au/substrate SPR mode—conveniently, without a spectrometer. In the last, we demonstrated the corrugated Au film was capable of sensing biomolecules, revealing the ability of the structure to be a highly sensitive biosensor.

1. Introduction

Rapid monitoring of environments can provide early warnings of dangerous surroundings. In situ sensing systems normally monitor changes in optical (Shi et al., 2010; Wan et al., 2010) or electronic (Mao et al., 2010; Zhu et al., 2009) signals, allowing us to quickly recognize variations in our environment. The most efficient method for monitoring environmental variation is to detect changes in the refractive index (RI) of the surrounding medium. A surface plasmon resonance (SPR) is a collected oscillation of charges at metal–dielectric interface, and its oscillation frequency is highly dependent on the RI of the surroundings. When the surrounding medium alters, thus the RI value, the SPR frequency will shift, providing information about the surrounding (Homola, 2006). For example, when biomolecules are adsorbed on the metal–dielectric interface, it would induce a local RI change, and thus change the SPR frequency. By monitoring the frequency change, we can perceive information about the biomolecules such as concentrations and species. With this unique phenomenon, the SPR is used widely in label-free biological and chemical sensing (Chabot et al., 2009; Chien et al., 2007; Pollet et al., 2009; Yanase et al., 2010). Typically, the SPR is excited using a prism coupler (Aslan and Geddes, 2009; Kim and Kihm, 2007; Svedendahl et al., 2009), highly focused laser beams, or sub-wavelength periodical metal structures (Avrutsky et al., 2000; Chang and Gray, 2005; Thio et al., 2000; Ye and Zhang, 2004, 2005) A prism coupler, normally with Kretschmann geometry (Kretschmann and Raether, 1968), is highly sensitive to the surrounding RI, with reported sensitivities of up to few thousand nanometers per refractive index unit (RIU) (Yu and Fan, 2011). A drawback of this method, however, is the complexity of its configuration. Sub-wavelength, periodical metal structures are alternative systems for exciting the SPR. For example, metallic hole arrays are efficient nanostructures for SPR excitation; they exhibit optically extraordinary transmission (EOT) (Ctistis et al., 2007; Ebbesen et al., 1998; Gao et al., 2006). The changes in RI of the surrounding medium cause the EOT to occur in different wavelength regimes. Therefore, monitoring the EOT induced by SPR provides information regarding the environmental RI. Nanohole arrays have been applied widely in chemical and biological sensors (Chen et al., 2009; Leebeeck et al., 2007; Menezes et al., 2010; Sharpe et al., 2008); for example, for detecting chemical solutions of unknown RIs. Moreover, label-free, real-time bio-probes have been developed based on metallic nanohole arrays (Ji et al., 2008; Yang et al., 2008). In addition, due to the unique plasmonic characteristics of nanohole structures, single-hole detection (Park et al., 2008; Rindzevicius et al., 2005) or in-hole detection (Ferreira et al., 2009) are also possible.

Other promising candidates for biological and chemical sensing are corrugated metal film structures. In a previous study, we used nanoimprint lithography to fabricate periodic, 1D corrugated metal

* Corresponding author. Tel.: +886 2 33664076; fax: +886 2 23634562.
E-mail address: hsuenlichen@ntu.edu.tw (H.-L. Chen).

0956-5663/$ – see front matter © 2012 Elsevier B.V. All rights reserved.
doi:10.1016/j.bios.2012.01.021

structures; the periodically corrugated metal films efficiently coupled the incident light into an SPR mode and contributed to the EOT (Chuang et al., 2008). By alternating the radius of curvature at the tip, the intensity of the EOT could be finely tuned. In addition, the SPR mode of the corrugated metal film was simplified, allowing the signal change to be readily observed and analyzed. Therefore, we suggest that corrugated metal film structures have great potential for use in highly sensitive chemical sensors.

Typically, the response of an SPR-based sensor to a change in the surrounding RI is indicated through a variation in the resonance wavelength or angle. Another unique optical response to a change in the surrounding RI is the variation in intensity of the EOT. We have found that the intensity of the EOT is influenced to a great extent by the coupling efficiency of the SPR mode into the other side of metal film; when the RIs on the two sides of the metal film are consistent, the coupling efficiency is optimized. Because of this unique index-matching phenomenon (Im et al., 2010; Krishnan et al., 2001), the intensity of the EOT increases as the RI of the superstrate approaches that of the substrate. Notably, the index-matching effect is a universal phenomenon, so any substrates can utilize this effect (in our case, we used PC substrate). Although this behavior suggests a new criterion for refractometric sensing, the change in intensity of the EOT is difficult to quantify. Therefore, although plasmonic sensors based on nanohole arrays (Chen et al., 2009; Leebeeck et al., 2007; Menezes et al., 2010; Sharpe et al., 2008) have demonstrated the refractometric sensing by the intensity of EOT, however, to the best of our knowledge, a quantified refractometric sensing, namely, a linear change in intensity of EOT relative to surrounding RI has not been reported previously.

In this study, we developed a plasmonic sensor based on a corrugated Au film structure by one-step of the nanoimprint-in-metal method. And we discussed in detail the plasmonic property of the corrugated Au film structure. By exploiting the plasmonic property of the corrugated Au film structure, we developed a biosensor accordingly. Due to excitation of the SPR mode, the corrugated Au film displayed high sensitivity (>800 nm/RIU). Moreover, it exhibited a quantifiable intensity change upon altering the surrounding RI. In the last, we demonstrated that the corrugated Au film could act as a biosensor for sensing cysteine in a concentration down to micromolar. With sensing capability based on both SPR and index-matching effects for determining surrounding refractive indices with high sensitivity and accuracy, corrugated Au films prepared using the nanoimprint-in-metal method are promising candidates for use as portable, disposable, and flexible chemical and biological sensors.

2. Materials and methods

2.1. Materials

All chemicals were used as received, without any further purification. Sodium citrate (99%), silver nitrate ($AgNO_3$, 99%), hydrogen tetrachloroaurate ($HAuCl_4$, 99.999%), copper nitrate [$Cu(NO_3)_2$, 98%], cysteine (Cys, 97%), polyvinylpyrrolidone (PVP; Mw 30,000), 1-hexadecanethiol, methanol (MeOH, 99.5%), ethanol (EtOH, 99.8%), and ethylene glycol (EG, 99.8%) were obtained from ACROS. Index matching oils (RI = 1.30–1.60) were purchased from Cargille-Sacher Laboratories Inc. PC substrates having a thickness of 365 μm were obtained from PERM TOP Co., Ltd.

2.2. Nanoimprint-in-metal

A 70-nm-thick Au film was first deposited on a polycarbonate (PC) substrate by a sputter system. A grating mold having a line width of 400 nm and period of 800 nm was fabricated by e-beam lithography. The imprint system was heated to the glass transition temperature (T_g) of the PC substrate (150 °C). The master mold and the Au film then came into contact under a moderate pressure (5–10 MPa), causing the Au film to deform into a corrugated morphology.

2.3. Cysteine target solution preparation

Gold nanoparticles were prepared through the reaction of $HAuCl_4$ with Ag NPs. Briefly, $AgNO_3$ (0.04 g) and PVP (1 g) were dissolved in EG (20 mL). This mixture was heated at 160 °C for 2 h under magnetic stirring and then cooled to room temperature. The resulting Ag colloid prepared using the polyol method formed stable dispersions in water without the need to add additional stabilizers. The solution of the Ag nanoparticles (1 mL) was diluted in deionized water (25 mL) and then heated under reflux for 10 min before 2 mM aqueous $HAuCl_4$ (1.5 mL) was added dropwise. After 20 min of stirring, the particles were cooled to room temperature, purified through gradient centrifugation, washed twice with 0.3 mM aqueous sodium citrate, redispersed in 0.3 mM sodium citrate (5 mL), and finally stored at 4 °C. The Cys-coated gold nanoparticle target solutions were freshly prepared by mixing Cys (1 mM–1 μM) and colloidal solution of gold nanoparticles (1:7, v/v) for 3 min.

2.4. Biosensing measurement

The as-fabricated samples were sequentially immersed in aqueous solutions of Cys (1 mM), Cu^{2+} (1 mM), and Cys-coated Au NPs (target solution, 1 mM–1 μM) for 10, 10, and 30 min, respectively. The Cys-coated Au NP target solution was prepared fresh prior to the immersion by mixing Cys (from 1 μM to 1 mM) and Au NPs (1:7, v/v) for 3 min. After performing a final rinse with ultrapure water, removing the unbinding target, the as-fabricated sample was dried under a flow of nitrogen. A flow chart of sample preparation and the optical measurement setup are displayed in Supplementary data, Figs. S1 and S2.

2.5. Characterization

The transmission spectra were measured using a Hitachi U4100 optical spectrometer. The light source is un-polarized. The corrugated structures were observed using a Hitachi S4000 scanning electron microscope (SEM).

3. Results and discussion

Fig. 1(a) presents a schematic illustration of the fabrication of a corrugated Au film structure through the direct nanoimprint lithography in metal. The period of the master mold defined the period of the corrugated Au film. Varying the applied pressure allowed fine control over the trench depth and the curvature of the tips of the corrugated Au film. Fig. 1(b) displays a scanning electron microscopy (SEM) image of one such structure. A large area of this Au film was deformed into a corrugated morphology, providing a uniform and periodic one dimensional (1D) structure. The inset to Fig. 1(b) presents a cross-sectional SEM image of the corrugated morphology of the as-fabricated sample. This periodically corrugated Au film could undergo excitation of the SPR and feature an EOT; moreover, the electric field would be concentrated at the sharp tips of the corrugated Au film. We used the three-dimensional finite difference time domain (3D-FDTD) method to analyze the electric field intensity distribution throughout the structure (Fig. 1(c)). Our simulations revealed that the electric field intensity was strong at

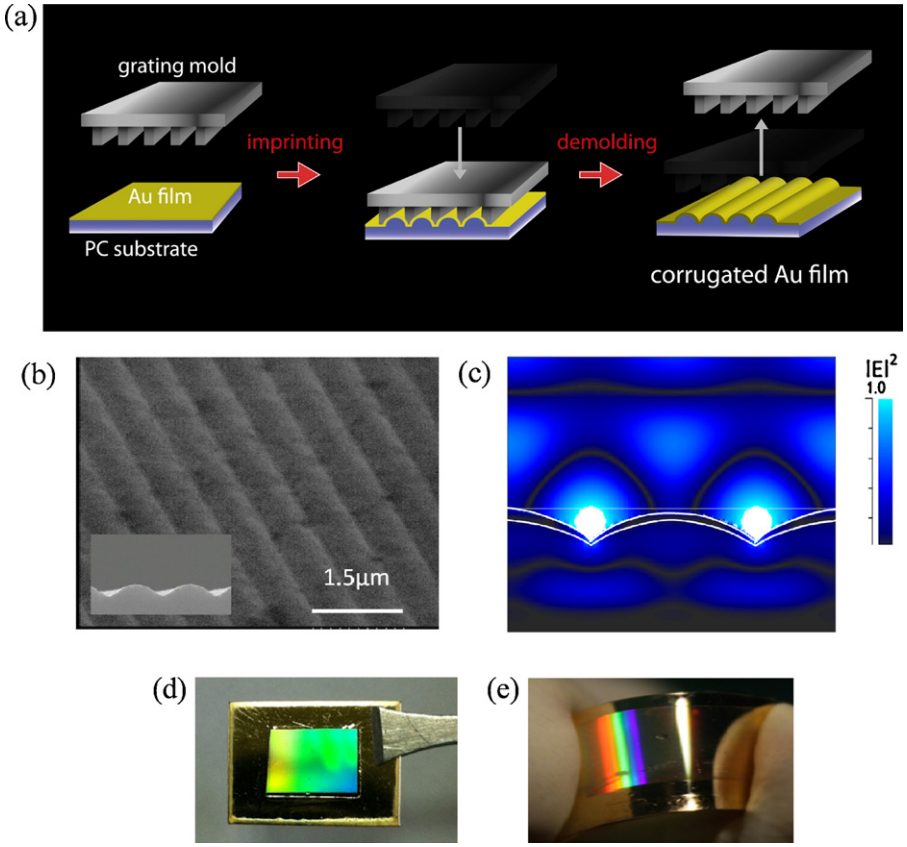

Fig. 1. (a) Schematic illustration of the fabrication of a corrugated Au film using the direct nanoimprint-in-metal method. (b) SEM image of a corrugated Au film. Inset: Cross-sectional SEM image. (c) 3D-FDTD simulated image of the corrugated Au film. (d and e) Photographs of (d) a corrugated Au film and (e) its highly flexible structure.

the tips of the structure, enabling the energy of the SPR to couple into the other side of the Au film, contributing to enhanced transmission. Fig. 1(d) and (e) presents photographic images of a chemical sensing chip based on such a corrugated Au film. The chemical sensing chip exhibited a colorful diffraction pattern because of the presence of the periodically corrugated nanostructures (Fig. 1(d)); it was also highly flexible (Fig. 1(e)). Because we fabricated our sensing chips on flexible plastic substrates using the one-step nanoimprint lithography method, the fabrication of such chips should be compatible with a roll-to-roll (R2R) process, allowing the preparation of large numbers of chemical sensing chips both rapidly and conveniently.

Next, we investigated the SPR modes of the corrugated Au film fabricated under an applied pressure of 8 MPa. We collected zero-order transmission spectra, measured with incident angles ranging from 0 to 60° at an increment of 1°, to form the dispersion diagram displayed in Fig. 2(a). The resonance wavelength of the SPR modes for a 1D periodical nanostructure under normal incidence can be defined using the equation:

$$\lambda_{SPR} = \frac{a}{|m|}\sqrt{\frac{\varepsilon_m \varepsilon_d}{\varepsilon_m + \varepsilon_d}} \quad (1)$$

where a is the period of the metallic structure, ε_m is the dielectric constant of Au, ε_d is the dielectric constant of the surrounding medium, and m represents the mode number of the SPR. Instead of featuring complicated multiple SPR modes, the corrugated Au film exhibited much simpler SPR modes in its dispersion diagram. The simplicity of the excited modes of corrugated metal films made it easy to perceived and analyze their SPR spectral changes. No additional analysis was required to clarify the implications of the signals in the measured spectra—enabling rapid and direct sensing.

To demonstrate the potential of using such corrugated Au films as biosensors, the plasmonic response to surrounding RI of the structure must be discussed. We first immersed a sensing chip based on the corrugated Au film into superstrates of different RIs (index matching oil, Cargille Labs; $n = 1.30$–1.60). Fig. 2(b)–(d) presents mappings of the index-dependent transmission spectra for corrugated Au films prepared under various applied pressures. Two SPR modes existed in the infrared ray (IR) regime. The first, in the longer wavelength regime, was the first SPR mode excited between the Au film and the PC substrate, denoted as the Au/PC mode ($m = 1$). This mode was difficult to observe in the ambient environment. Increasing the value of n_{sup}, however, allowed the Au/PC mode to become clearly identifiable as a result of the index-matching phenomenon. The other SPR mode, revealed in the shorter wavelength regime, was the first SPR mode between the Au film and the superstrate, denoted as the Au/sup mode ($m = 1$). When the value of n_{sup} increased from 1.30 to 1.55, the Au/sup SPR mode underwent an obvious red-shift, from ca. 1090 nm to 1240 nm. In contrast, the Au/PC SPR mode did not undergo any wavelength-shift because of the unchanged RI of the substrate. The imprinting pressure influenced the morphology of the corrugated Au film in terms of the curvature of the structure tips. Higher imprinting pressures led to larger curvature at the tips; such sharper tips led to greater concentration of the electric field at the tips, causing the energy of the Au/sup SPR mode to couple into the Au/PC mode more efficiently. Therefore, for a structure with small curvature, the Au/sup SPR mode could couple to the Au/PC mode only under index-matching conditions—that is, when the value of n_{sup} was close to that of n_{sub}. On the other hand, when the structure featured large curvature at its tips, the energy of the Au/sup mode readily coupled into the Au/PC mode through the sharp tips because of the enhanced electric field intensity. As indicated in Fig. 2(b), when the

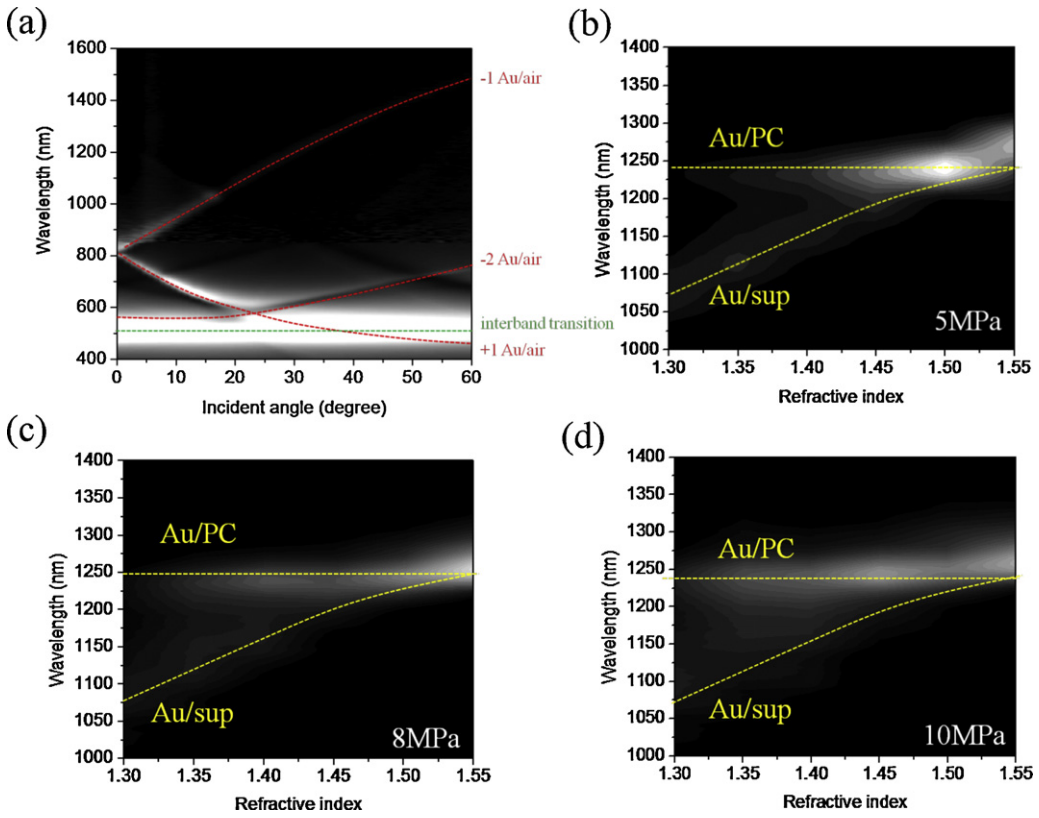

Fig. 2. (a) SPR dispersion diagram of the corrugated Au film having a period of 800 nm. Index-dependent transmission mappings of corrugated Au films that had been prepared using applied pressures of (b) 5 MPa, (c) 8 MPa, and (d) 10 MPa.

corrugated Au film was fabricated under a lower applied pressure (e.g., 5 MPa), the energy coupling between the two modes was less efficient for smaller values of n_{sup} regime, but became obvious when the value of n_{sup} approached that of n_{sub}. As expected, the energy coupling of the two modes became more apparent for the corrugated Au films fabricated under higher pressure, even for lower values of n_{sup} (Fig. 2(c) and (d)). For example, the corrugated Au films fabricated under pressures of 8 and 10 MPa had its two modes begin to couple at values of n_{sup} of 1.32 and 1.30, respectively. The coupling was so efficient even when there was a difference of ca. 0.2 RIU between the values of n_{sup} and n_{sub}. Noticeably, we observed an interesting phenomenon in the three mappings: the intensity of the Au/PC mode increased upon increasing the value of n_{sup} for the three corrugated Au films, regardless of the applied pressure during fabrication.

Fig. 3(a) displays typical transmission spectra for a corrugated Au film at different values of n_{sup}. The index-matching phenomenon was strongly evident in the transmission intensity of the Au/PC mode. When the RIs of the superstrate and substrate were identical, the Au/sup mode efficiently coupled into the Au/PC mode, resulting in a larger transmission intensity. The transmission intensity of the Au/PC mode increased linearly upon increasing the value of n_{sup}, reaching its maximum at a value of n_{sup} of 1.55 (equal to the RI of the underlying PC substrate). Moreover, the transmission intensity dropped when we further increased the value of n_{sup} to 1.60, a direct consequence of the mismatch between the values of n_{sup} and n_{sub}. Thus, the transmission intensity of the Au/PC mode was highly dependent on the index-matching effect. This unique phenomenon suggested that the transmission intensity of the Au/PC mode could be an additional criterion, beside the wavelength-shift of the SPR mode, for refractometric sensing. Notably, refractometric sensing based on the index-matching effect of the Au/PC mode is much more convenient than using the conventional SPR wavelength shift, which typically requires a spectrometer to scan over the whole spectrum. In contrast, the Au/PC mode we applied here for refractometric sensing is monitored at a fixed SPR wavelength (ca. 1250 nm). Therefore, the latter approach does not need an expensive spectrometer scanning over the entire spectrum, but rather only a light source and a photodetector to monitor the change in intensity of the Au/PC mode. Thus, this method could provide more-convenient, faster, cheaper, and simpler refractometric sensing. Next, we used the 3D-FDTD method to simulate the index-matching effect. The corrugated Au film in simulation was designed as the real one in experiment. The substrate was PC (RI = 1.55), and superstrates having RI of 1.00 and 1.55 were used in the simulation. The incident wavelength was set to 1250 nm, and the white arrow indicated the incidence direction. The morphology of structure was outlined by white line and colors in the simulated images indicated the amplitude of electric field. As indicated in Fig. 3(b), when the RI of superstrate was 1.00, far from that of PC substrate, the index-matching effect was not obvious, and thus the transmitted intensity was low. The enhancement of local electric field intensity achieved its maximum when the RI of superstrate was identical to that of substrate. As displayed in Fig. 3(c), there was strong electric field intensity at the tips of the corrugated Au film, and the transmitted intensity was much larger than that in Fig. 3(b). From the near-field simulation, it was evident that the index-matching effect could result in much different transmission of Au/PC SPR mode, and confirmed that this unique phenomenon was much quantified in the corrugated Au film compared to other periodic metallic structure reported.

Fig. 4(a) displays the dependence of the resonance wavelength shift on the value of n_{sup} for sensing chips incorporating corrugated Au films. The calibration curves, with linear equation and correlation coefficient (r) provided in the figure, displays the highly linear relationships between the resonance wavelengths and the values

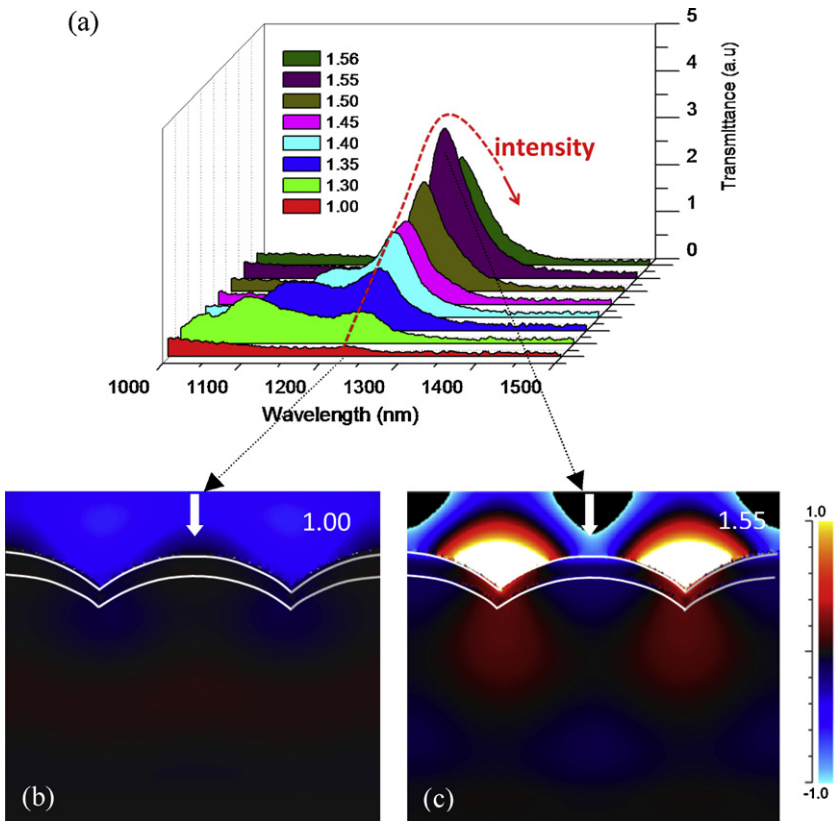

Fig. 3. (a) Transmission spectra of a corrugated Au film (period: 800 nm; pressure: 8 MPa) in the presence of superstrates of various RIs. (b and c) 3D-FDTD simulated images of the corrugated Au film in the presence of superstrates having RI of (b) 1.00, and (c) 1.55, respectively. White arrows indicated the direction of incident light. (For interpretation of the references to color in text, the reader is referred to the web version of the article.)

of n_{sup} (surrounding RI). The slopes of these calibration curves corresponded to the sensitivity, which we defined using the equation

$$S_\lambda = \frac{\Delta\lambda}{\Delta n} \tag{2}$$

where S_λ is the sensitivity determined by the shift in the resonance wavelength (units: nm/RIU). The three corrugated Au films, with their different curvatures at their tips, performed with similarly sensitivity and with linear responses to the values of n_{sup}. The corrugated Au films fabricated at 5, 8, and 10 MPa exhibited high sensitivities of 812, 753, and 748 nm/RIU, respectively. The high sensitivity of these as-fabricated sensors means that slight changes in surrounding RI could be detected simply.

In addition to the sensitivity determined by shifts in the resonance wavelength, we also demonstrated a sensing criterion based on the intensity of the EOT. Fig. 4(b) summarizes the index-dependent variations of the intensities of the EOT. Similar to the shifts in the resonance wavelengths, the variation of the EOT intensity also followed approximately linear calibration curves. Therefore, the sensitivity based on intensity could be defined using the equation

$$S_T = \frac{\Delta T}{\Delta n} \tag{3}$$

where S_T is the sensitivity determined by the intensity of the EOT [units: absolute units (a.u.) per RIU]. For the corrugated Au films prepared at 5, 8, and 10 MPa, the values of S_T were approximately 6.25, 8.96, and 5.21 a.u./RIU, respectively. A slight difference in the value of S_T for corrugated Au film prepared at different pressures, but a highly linear response could be observed for each one as well. This change in intensity provides another criterion for determining the RIs of unknown superstrates. Thus, the corrugated Au films provided dual criteria for refractometric sensing: one based on the wavelength shift of the Au/sup mode exhibited high sensitivity (comparable with or even higher than those of other previously reported SPR-based sensors); the other, based on the change in the EOT intensity of the Au/PC mode, exhibited a highly linear response to the surrounding RI. To the best of our knowledge, no other SPR-based sensors exhibiting such a response of the EOT intensity to the surrounding RI have been applied to refractometric sensing. Employing dual criteria for refractometric sensing will clearly provide more-accurate sensing data. The RI determined by each of the two criteria could be examined independently, minimizing experimental errors during sensing.

To demonstrate the potential applications of the corrugated Au film for refractometric sensing, we used a corrugated Au film to determine the RIs of aqueous solutions incorporating EtOH at different concentrations. Fig. 5(a) presents transmission spectra of a corrugated Au film immersed in each of the aqueous EtOH solutions. The resonance wavelength of the Au/sup mode underwent a red-shift upon increasing the concentration of EtOH in the aqueous solution. The resonance wavelength shifted by ca. 20 nm when the superstrate varied from deionized water (DIW) to 99% EtOH. The theoretical change in RI for these solutions (Lide, 2011) is approximately 3×10^{-2} RIU—a relatively small change to be perceived. Our chemical sensor based on a corrugated Au film demonstrated a recognizable signal change, namely an obvious shift in wavelength in the transmission spectra. We fitted the measured resonance wavelength shifts (Au/sup mode) to the calibration curves derived from Fig. 4(a) and calculated the corresponding RIs accordingly (Fig. 5(b)). The RIs calculated from the shift in resonance wavelength were in a good agreement with the reference RIs. The refractive index of each EtOH solution was predicted precisely by this chemical sensor based on a corrugated Au film. The

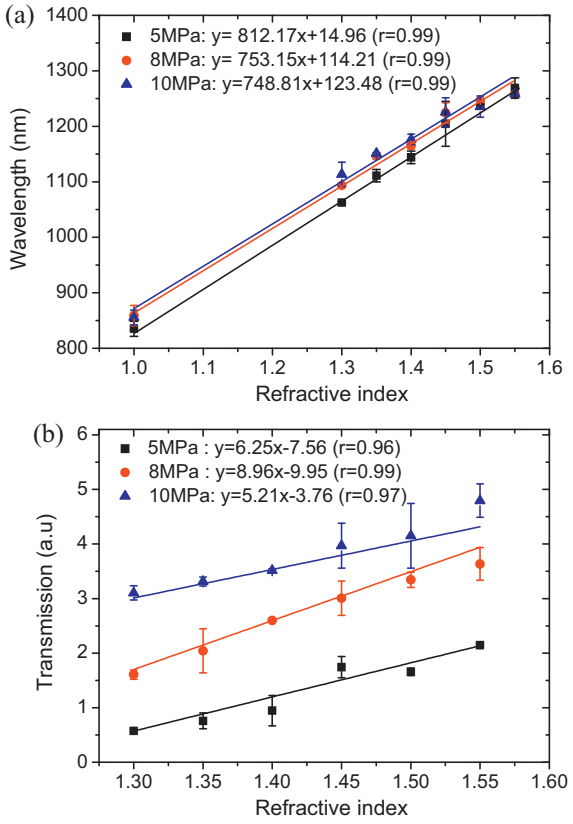

Fig. 4. Linear calibration curves of the RI-dependent (a) SPR wavelength of the Au/sup mode and (b) transmission intensity of the Au/PC mode.

average error was on the order of 10^{-3} RIU, implying highly accurate sensing.

In addition, to detect such slight variations in the RIs of EtOH solutions, we can use solutions of known RIs—in our case, the DIW and 99% EtOH solution—as standard superstrates and then take the corresponding transmission intensities of the Au/PC mode to interpolate the RIs of aqueous EtOH solutions having intermediate concentrations. Fig. 5(c) reveals that the RIs determined from the transmission intensity of the Au/PC mode were also consistent with the reference data. The maximum mismatch between the calculated and reference RIs was less than 10^{-3} RIU, indicating the high reliability of this method. Fig. 5(d) plots the RIs averaged from the data determined from the SPR wavelength-shift and from the transmission intensity of the Au/PC mode. The calculated RIs were coincident with the reference values, with the mismatch error further reduced to ca. 10^{-4} RIU. Therefore, by mutually examining the RIs determined from the shift in the SPR wavelength and the transmission intensity of the Au/PC mode, we could exclude some experimental errors and obtain more-accurate data. We conclude that our chemical sensors for refractometric sensing, based on dual sensing criteria, were highly sensitive and accurate. Besides, the rapid response of an as-fabricated sensor could be seen through in situ monitoring of the shift in the SPR wavelength (Au/sup mode) and of the transmission intensity of the Au/PC SPR mode during liquid flow tests (Supplementary data, Fig. S3). Therefore, this chemical sensor based on a corrugated Au film could allow accurate and rapid monitoring of environmental RIs within a relatively short response time.

Besides sensing chemical solutions, a corrugated Au film was capable to sense biomolecules as well. We used the corrugated Au film as a biosensor to detect cysteine (Cys). Cys is a thiol-containing amino acid that played an important role in many diseases.

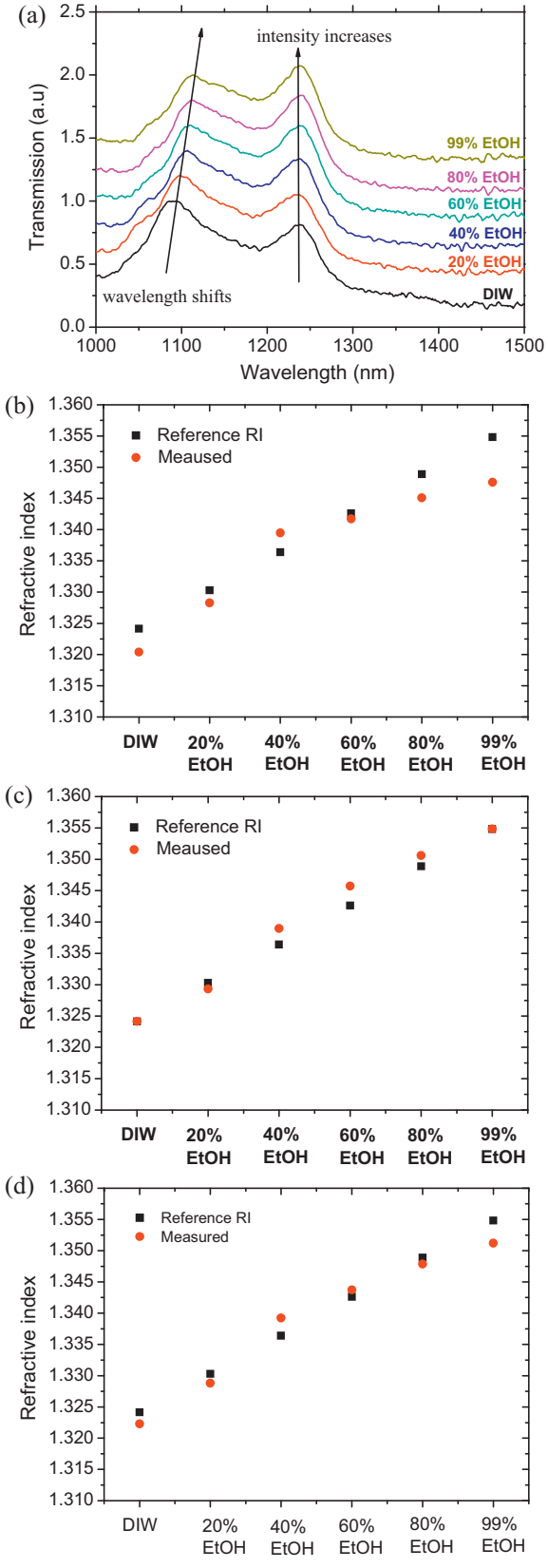

Fig. 5. (a) Transmission spectra of a corrugated Au film (period: 800 nm; pressure: 8 MPa) immersed in aqueous EtOH solutions of different concentrations. (b and c) Comparison of the reference RIs with those determined from (b) the SPR wavelength of the Au/sup mode and (c) the transmission intensity of the Au/PC mode. (d) Average values of the RIs in (b) and (c).

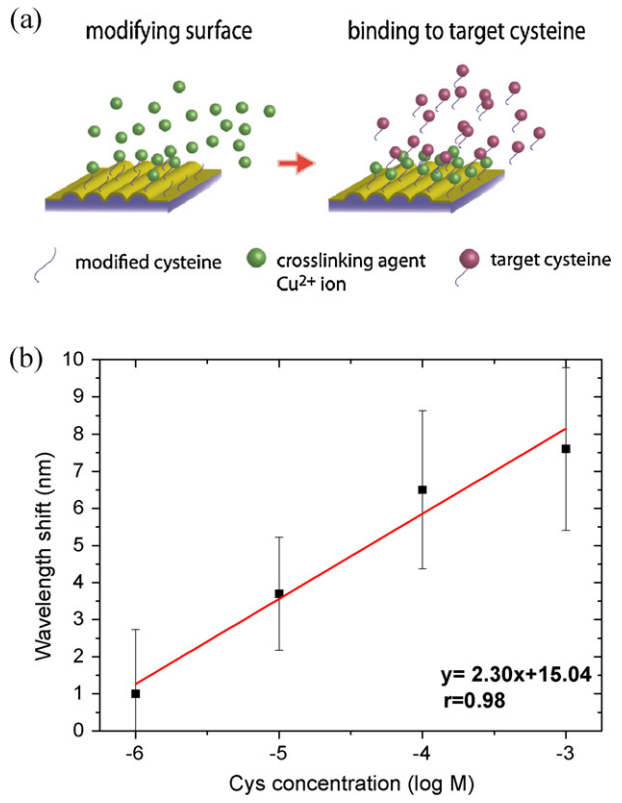

Fig. 6. (a) Schematic illustration of Cys-detection technique based on the corrugated Au film. (b) Dependence of the resonance wavelength shift of Au/sup mode on the concentrations of target Cys solutions.

Therefore, Cys-detection technique had a wide application in biological and medical science. Fig. 6(a) displays the schematic illustration of the Cys-detection technique based on a corrugated Au film. We first modified the surface of corrugated Au film with a monolayer of Cys molecules. Then, the surface-modifying Cys molecules were further bound to Cu^{2+} ions at the end of molecular chain. Cu^{2+} ions served as crosslinking agent that bound to target Cys molecules in the next step of biosensing. Various concentrations of target Cys solutions were prepared for the detection. Fig. 6(b) displays the dependence of the resonance wavelength shift on the concentrations of target Cys solutions. As indicated in Fig. 6(b), the relationship between the resonance wavelength shift and concentrations of target Cys solutions is linear. On the other hand, the corrugated Au film still performed a high sensitivity to small amount of Cys molecules. The SPR wavelength shift was ca. 1 nm for the 10^{-6} M of target solution concentration. The experimental results suggested that the corrugated Au film possessed the capability of sensing small amount of biomolecules.

4. Conclusions

In this study, we prepared metallic corrugated structures for application as SPR based biosensors. Relying on a one-step nanoimprint-in-metal method, the fabrication of these SPR-based sensors was much simpler than that of traditional approaches using lithography and etching processes. Plasmonic sensors based on the corrugated Au films exhibited high sensitivity (ca. 800 nm/RIU), comparable with or even higher than those of other SPR-based sensors. Because of the unique index-matching effect, refractometric sensing could be determined by monitoring the transmission intensity of the Au/PC SPR mode; such measurements can be performed conveniently without the need for a spectrometer. In addition, the two criteria for sensing—based on the shift of the SPR wavelength and the transmission intensity—allowed mutual examination of the sensing results. In the last, we demonstrated the corrugated Au film was capable to be a highly sensitive biosensor. And therefore, the plasmonic sensor has several advantageous properties: simple fabrication, high sensitivity, dual-criteria monitoring, accurate and rapid sensing, and the potential to be incorporated in disposable chemical and biological sensors.

Acknowledgment

We thank the National Science Council, Taiwan and Chung-Shan Institute of Science and Technology, for supporting this study under contracts NSC-100-2628-E-002-031-MY3, NSC 100-2628-E-002-023-MY2, and CSIST 100-EC-17-D-02-11-1057.

Appendix A. Supplementary data

Supplementary data associated with this article can be found, in the online version, at doi:10.1016/j.bios.2012.01.021.

References

Aslan, K., Geddes, C.D., 2009. Anal. Chem. 81, 6913–6922.
Avrutsky, I., Zhao, Y., Kochergin, V., 2000. Opt. Lett. 25, 595–597.
Chabot, V., Cuerrier, C.M., Escher, E., Aimez, V., Grandbois, M., Charette, P.G., 2009. Biosens. Bioelectron. 24, 1667–1673.
Chang, S.H., Gray, S.K., 2005. Opt. Express 13, 3150–3165.
Chen, J., Shi, J., Decanini, D., Cambril, E., Chen, Y., Haghiri-Gosnet, A.M., 2009. Microelectron. Eng. 86, 632–635.
Chien, F.C., Lin, C.Y., Yih, J.N., Lee, K.L., Chang, C.W., Wei, P.K., Sun, C.C., Chen, S.J., 2007. Biosens. Bioelectron. 22, 2737–2742.
Chuang, S.Y., Chen, H.L., Kuo, S.S., Lai, Y.H., Lee, C.C., 2008. Opt. Express 16, 2415–2422.
Ctistis, G., Patoka, P., Wang, X., Kempa, K., Giersig, M., 2007. Nano Lett. 7, 2926–2930.
Ebbesen, T.W., Lezec, H.J., Ghaemi, H.F., Thio, T., Wolff, P.A., 1998. Nature 391, 667–669.
Ferreira, J., Santos, M.J.L., Rahman, M.M., Brolo, A.G., Gordon, R., Sinton, D., Girotto, E.M., 2009. J. Am. Chem. Soc. 131, 436–437.
Gao, H., Henzie, J., Odom, T.W., 2006. Nano Lett. 6, 2104–2108.
Homola, J. (Ed.), 2006. Surface Plasmon Resonance Based Sensors. Springer, Berlin.
Im, H., Lindquist, N.C., Lesuffleur, A., Oh, S.H., 2010. ACS Nano 4, 947–954.
Ji, J., O'Connell, J.G., Carter, D.J.D., Larson, D.N., 2008. Anal. Chem. 80, 2491–2498.
Kim, I.T., Kihm, K.D., 2007. Anal. Chem. 79, 5418–5423.
Kretschmann, E., Raether, H., 1968. Z. Naturforsch. A: Astrophys. Phys. Phys. Chem. A23, 2135–2136.
Krishnan, A., Thio, T., Kim, T.J., Lezac, H.J., Ebbesen, T.W., Wolff, P.A., Pendry, J., Martin-Moreno, L., Garcia-Vidal, F.J., 2001. Opt. Commun. 200, 1–7.
Leebeeck, A.D., Kumar, L.K.S., de Lange, V., Sinton, D., Gordon, R., Brolo, A.G., 2007. Anal. Chem. 79, 4094–4100.
Lide, D.R., 2011. CRC Handbook of Chemistry and Physics, 91st ed. CRC Press, Boca Raton, FL.
Mao, S., Lu, G., Yu, K., Bo, Z., Chen, J., 2010. Adv. Mater. 22, 3521–3526.
Menezes, J.W., Ferreira, J., Santos, M.J.L., Cescato, L., Brolo, A.G., 2010. Adv. Funct. Mater. 20, 3918–3924.
Park, T.H., Mirin, N., Lassiter, J.B., Nehl, C.L., Halas, N.J., Nordlander, P., 2008. ACS Nano 2, 25–32.
Pollet, J., Delport, F., Janssen Kris, P.F., Jans, K., Maes, G., Pfeiffer, H., Wevers, M., Lammertyn, J., 2009. Biosens. Bioelectron. 25, 864–869.
Rindzevicius, T., Alaverdyan, Y., Dahlin, A., Hook, F., Sutherland, D.S., Kall, M., 2005. Nano Lett. 5, 2335–2339.
Sharpe, J.C., Mitchell, J.S., Lin, L., Sedoglavich, N., Blaikie, R.J., 2008. Anal. Chem. 80, 2244–2249.
Shi, W., He, S., Wei, M., Evans, D.G., Duan, X., 2010. Adv. Funct. Mater. 20, 3856–3863.
Svedendahl, M., Chen, S., Dmitriev, A., Kall, M., 2009. Nano Lett. 9, 4428–4433.
Thio, T., Lezec, H.J., Ebbesen, T.W., 2000. Physica B 279, 90–93.
Wan, D.H., Chen, H.L., Lai, Y.T., Yu, C.C., Lin, K.F., 2010. Adv. Funct. Mater. 20, 1742–1749.
Yanase, Y., Araki, A., Suzuki, H., Tsutsui, T., Kimura, T., Okamoto, K., Nakatani, T., Hiragun, T., Hide, M., 2010. Biosens. Bioelectron. 25, 1244–1247.
Yang, J.C., Ji, J., Hogle, J.M., Larson, D.N., 2008. Nano Lett. 8, 2718–2724.
Ye, Y.H., Zhang, J.Y., 2004. Appl. Phys. Lett. 84, 2977–2979.
Ye, Y.H., Zhang, J.Y., 2005. Opt. Lett. 30, 1521–1523.
Yu, Z., Fan, S., 2011. Opt. Express 19, 10029–10040.
Zhu, H., Wang, Y., Li, B., 2009. ACS Nano 3, 3110–3114.